ELSEVIER

Materials Science and Engineering A345 (2003) 223–233

MATERIALS SCIENCE & ENGINEERING A

www.elsevier.com/locate/msea

Micro-indentation and inverse analysis to characterize elastic–plastic graded materials

Yu Gu [a], Toshio Nakamura [a,*], Lubos Prchlik [b], Sanjay Sampath [b], Jay Wallace [c]

[a] *Department of Mechanical Engineering, State University of New York at Stony Brook, Stony Brook, NY 11794, USA*
[b] *Department of Materials Science and Engineering, State University of New York at Stony Brook, Stony Brook, NY 11794, USA*
[c] *National Institute of Standards and Technology, MATLS A256, Gaithersburg, MD 20899, USA*

Received 7 March 2002; received in revised form 24 June 2002

Abstract

Properties of actual graded materials were characterized with a new procedure based on inverse analysis. This procedure utilizes indirect experimental records obtained from instrumented micro-indentation and extracts key properties of indented specimen through the *Kalman filter* technique. The graded material is composed of mixture of Yittria Partially Stabilized Zirconia (PSZ) and NiCrAlY and it possesses varying elastic–plastic properties through its thickness. This procedure enables determination of the compositional profile and the effective mechanical property without resorting to complex experimental measurements. It relies solely on the load–displacement records of instrumented spherical indentation and the inverse analysis during the post-processing. The graded specimens were fabricated by plasma spray deposition process under controlled feeding of PSZ and NiCrAlY powders. Prior to testing of the graded materials, single phased coatings were made with each component and analyzed. This process allows consistent material constants to be used in the graded material analysis. Here PSZ and NiCrAlY were assumed to be elastic and elastic–plastic, respectively. The elastic moduli of both materials were estimated with a common indentation method while the plastic properties of NiCrAlY were determined by modifying the inverse method proposed for the graded materials. The latter procedure represents a new indentation method for characterization of homogeneous elastic–plastic materials. Once the properties of constituents were identified, the properties of graded material were estimated with the *Kalman filter* technique. The indented load–displacement relations simulated from finite element analysis with the estimated properties and that of measured record showed excellent agreement, which assures a high degree of accuracy in the current measurement procedure.

Keywords: Functionally graded material (FGM); Plasma sprayed coating; Micro-indentation; Inverse analysis; Kalman filter; Elastic–plastic material properties

1. Introduction

Graded materials or functionally graded materials (FGM) are increasingly being considered in various applications to maximize strengths and integrities of many engineering structures. In graded materials, compositions of multiple phases are varied through the body to fulfill specific functions. For example, they are designed to enhance protection of components from thermal shock and high strain rate loading and to increase wear resistance [1]. Techniques to fabricate graded materials include adhesive bonding, sintering, thermal spray and reactive infiltration [1,2]. In coatings and thin structures, compositions of multiple phases are varied along the thickness direction. This graded feature is essential to achieve required functions. However, this unique feature (e.g. graded layer) also makes the property evaluation very difficult. In the past, several methods have been presented to characterize properties of FGM's. Weissenbek et al. [3] defined the rule of mixtures for a ceramic/metal system. Suresh et al. [4] and Giannakopoulos and Suresh [5,6] developed analytical and experimental tools to estimate the elastic properties of graded materials using instrumented micro-indentation. Liu et al. [7] used elastic wave and progressive-

* Corresponding author. Tel.: +1-631-632-8312; fax: +1-631-632-8544
E-mail address: toshio.nakamura@sunysb.edu (T. Nakamura).

0921-5093/02/$ - see front matter
PII: S0921-5093(02)00462-8

learning neural network to determine material properties of FGM plates. Although these methods have led to improved FGM characterization, they were applicable to only elastic FGMs.

Recently, several methods that use instrumented indentation have been presented to determine elastic–plastic material properties of thin film and coatings. Although not for graded materials, Suresh and Giannakopoulos [8,9] introduced effective procedures to examine the residual stresses and elastic–plastic properties of homogeneous materials with micro-indentation records. Guidelines and assumptions needed for accurate measurements were also discussed in Refs. [10,11]. More recently, Dao et al. [12] utilized the forward–reverse method and instrumented sharp indentation to characterize elastic–plastic properties. For graded materials, Nakamura et al. [13] proposed an inverse analysis procedure based on the Kalman filter and instrumented micro-indentation.

In a complex material and structural system, direct measurements of unknown variables can be difficult and one has to infer or estimate the unknown state variables via indirect measurements of other measurable parameters. For example, in the current analysis, the FGM properties cannot be quantified without resorting to cumbersome techniques. The indirect estimation of essential FGM parameters requires a use of an 'inverse analysis technique' where unknown variables are sought via indirect measurements of indentation. Although many inverse analysis techniques have been introduced in various applications, the techniques are not effective unless they satisfy convergence and consistency conditions. In many cases, direct applications of inverse analysis techniques would not yield accurate solutions since many problems are ill-conditioned (i.e. difficult to converge to unique solution), and some known or presumed conditions must be prescribed to establish a robust procedure for individual cases.

Although the robustness and accuracy of this procedure was tested previously, it was done with computational models. In the present study, the inverse analysis procedure was applied to actual elastic–plastic graded specimens, as well as to the elastic–plastic homogeneous specimens. The FGM was fabricated as thermal barrier coatings (TBC's) using plasma spray technique. They are composed of yittria partially stabilized zirconia (PSZ) and metallic bond coat (NiCrAlY). To determine the properties of individual constituent, coatings made of either PSZ or NiCrAlY were tested initially. Though the procedure was earlier outlined in the computational analysis [13], actual implementation of the technique to real specimens required further tuning of the procedure. These necessary steps as well as the effectiveness of this measurement procedure are discussed in the present paper.

2. Experimental procedure

2.1. Specimen fabrication

All coatings were prepared using PT-F4MB plasma gun in the Center for Thermal Spray Research at Stony Brook. Ceramic and metallic single layered coatings were deposited onto mild steel substrates using Metco 204NS (PSZ) and Praxair Ni-346-1 (NiCrAlY) powders, respectively. The thickness of each PSZ and NiCrAlY layer is 0.5 and 0.4 mm, respectively. Same powders and the spraying setup were used for the FGM preparation. The processing details and spraying conditions are described in Ref. [14]. The spraying conditions were adjusted so that the microstructures of the ceramic and metallic phases within the FGM were same as those in single layered coatings as shown in Fig. 1(a). The linear grading was selected as the targeted composition variation. Using image analysis and/or X-ray diffraction techniques, the average variation from the linear profile was typically measured less than 5 wt.% [14]. In our present work, an image analysis program was utilized to process the micrograph to determine the volume fractions of NiCrAlY along several depths. The volume variation through-thickness is shown in Fig. 1(b). Here the compositions are measured as 100%NiCrAlY–0%PSZ at the interface and 20%NiCrAlY–80%PSZ at the surface. The overall volume variation through-thickness is nearly linear as was targeted. Nevertheless, local deviations can be sometimes larger due to the intrinsic characteristics of the spraying process. Prior to

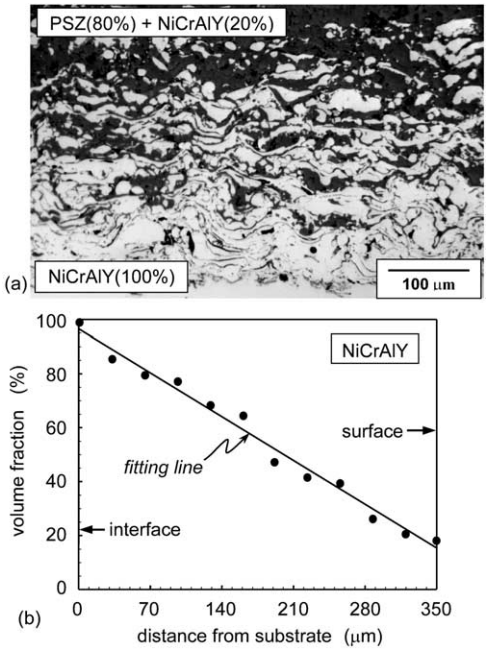

Fig. 1. (a) Micrograph showing cross-section of thermally sprayed graded coating. (b) Through-thickness variation of NiCrAlY volume by an image analysis. The straight line was obtained by least-square fit.

the indentation testing, the coating surfaces were polished using fine emery papers (240, 320 and 600 grit) and diamond suspensions (9, 3 and 1 μm). The total FGM thickness was measured as $t = 0.35$ mm. The surface roughness of all coatings was measured by the optical Zygo profilometer and found to be less than 0.08 μm.

2.2. Indentation test

The indentation was carried out using two different measurement systems to confirm the independence of the results from the testing setup and indenter material used. The first device used was a commercially supplied tester 'Nanotest 600' equipped with 'Micro-head' allowing the measurements up to 20 N maximum load (Micro Materials Ltd., Wrexham Technology Park, Wrexham LL13 7YP, UK) installed at the Massachusetts Institute of Technology. This instrument is equipped with a special electromagnetic force sensor and the displacement is measured indirectly by capacitance sensor mounted on the back of the indenter holder. The compliance of the indenter holder and the moving stage is measured prior to testing and subtracted from the experimental data measured. The compliance value in the setup was 0.35 μm N^{-1}. A spherical 440C steel indenter ($R = 0.8$ mm) was used in connection with this device. The second instrument was a modified microhardness tester installed in National Institute of Standards and Technology, which used a standard strain gage load cell for force measurements and a pair of capacitance sensors placed adjacent to the indenter for displacement measurements. The configuration and detailed description of the tester can be found, for example, in Ref. [15]. Two carbide–cobalt tungsten indenters with different diameters ($R = 0.8$ and 2.4 mm) were used in this experimental setup. The Young's modulus and Poisson ratio were $E^{440C} = 210$ GPa, $\nu^{440C} = 0.33$ and $E^{WC-Co} = 614$ GPa, $\nu^{WC-Co} = 0.22$ for hardened steel and WC–Co indenters, respectively. These values were used in the finite element calculations. Tabor suggested a simple criterion to estimate the onset of plastic deformation in the Brinell testing balls: the hardness of the indenter should be at least 2.5 times higher than that of material tested [16]. This was satisfied for both indenters and all materials tested. Moreover, the maximum load applied in the current tests ($P_{max} = 10$ N) was well below fully plastic regime considered in Tabor's criterion.

Prior to testing of FGM specimen, each constituent (i.e. PSZ and NiCrAlY) was tested separately to measure its individual properties. Fig. 2(a and b) depict the testing configuration for PSZ and NiCrAlY, respectively. For the measurement of these homogeneous specimens, single indenter record ($R = 0.8$ mm) was used in the inverse analysis to estimate their properties.

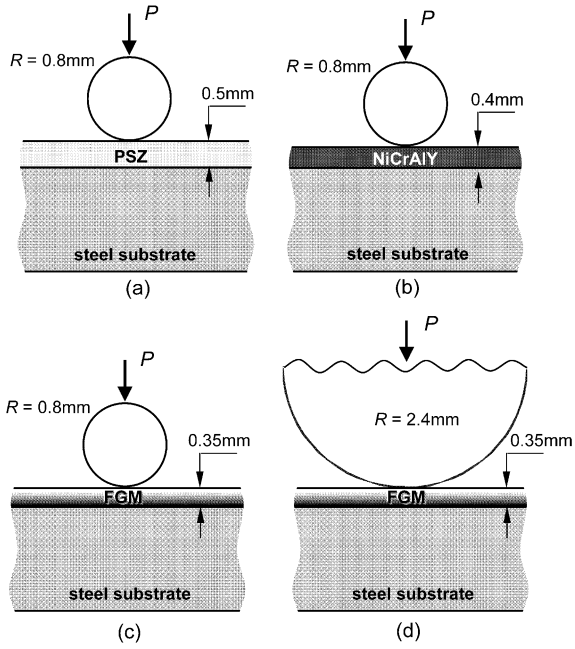

Fig. 2. Micro-indentations of coatings are illustrated for: (a) PSZ; (b) NiCrAlY; (c) FGM with small indenter; and (d) FGM with large indenter. The thickness of steel substrate is 2 mm in all cases.

For the FGM specimens, load–displacement records from multiple indenters were employed. In the previous study [13], it was found that results from two differently sized indenters significantly improved the convergence characteristics of unknown parameters. With an extra indenter of different radius, additional information regarding to the compositional gradient can be gained. This is possible since the sizes for zone of influence underneath the indentation are different for the two indenters and the length-scale effect of the FGM (i.e. grading/thickness) implicitly appears in their records. However, unlike the FGM, an extra indenter does not offer useful information for homogeneous materials since the length-scale is not relevant in their property description. The indenters with two different radii ($R =$ 0.8 and 2.4 mm) used for the FGM are schematically illustrated in Fig. 2(c and d), respectively. The size difference of 300% should be sufficient for producing different in characteristics their P–Δ records.

In general, it is desirable use indenters whose radii are comparable in size to the coating thickness. Measurements from a large indenter can include the effects of substrate and approximations based on Hertz contact solution may not be valid. In the present study, somewhat larger indenters had to be used since smaller sized indenters were not available. However, these indenters did not cause inaccuracies during the property determinations since independent finite element solutions,

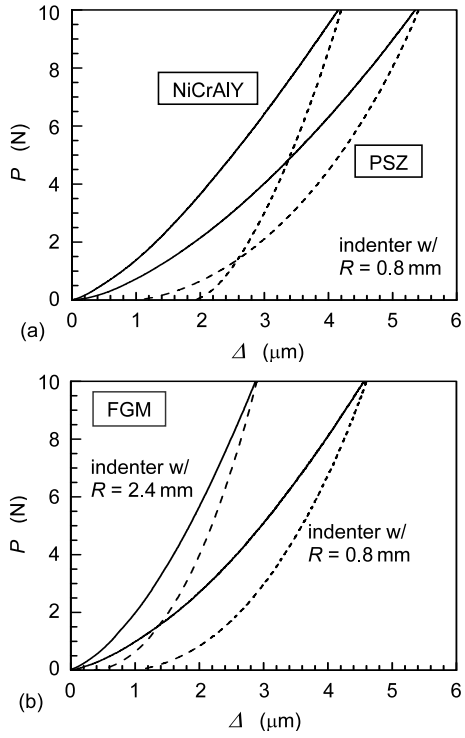

Fig. 3. Experimentally measured load–displacement records from micro-indentation for: (a) PSZ and NiCrAlY with indenter $R = 0.8$ mm; and (b) FGM with indenters $R = 0.8$ and 2.4 mm. Each curve represents average of about 10 indentations. The unloading records are shown with dashed lines.

where the indenter and substrate were modeled in exact dimensions, were used to compare with the measurements. Measured load–displacement records of the three different coatings are shown in Fig. 3. In each case, at least 10 tests were conducted and the averaged P–Δ record is shown. The figures show the loading up to 10 N and subsequent unloading to zero force. For NiCrAlY and FGM, the maximum load level was selected based on previous analysis [13] and their estimated yield strength, so that the indentation would cause a sufficient amount of plastic flow. Without plastic deformation, their plastic properties could not be determined. In fact, large residual indented displacement after complete unloading observed for NiCrAlY, shown in Fig. 3(a), is due to residual plastic strain. Note that the small amount of residual displacement observed for PSZ was not due to plastic flow but rather attributed to compaction or crashing during indentation. For FGM measurements, the larger indenter showed stiffer response due to its larger indented area as shown in Fig. 3(b). Both small and large indenters exhibit smaller residual displacement than that of NiCrAlY after unloading.

3. Inverse analysis procedure

3.1. Kalman filter

The present inverse analysis utilized Kalman filter technique [17] to estimate the unknown material properties. The procedure has been described extensively in Ref. [13] and only brief outline is given here although specifics needed to perform this analysis on real specimens are noted. This technique processes experimentally obtained data and attempts to obtain best estimates of unknown material constants. Essentially the Kalman filter algorithm updates the previous estimates through indirect measurements of unknown state variables and covariance information of both the state and measurement variables. In our analysis, indented displacement $\boldsymbol{\Delta\Omega}$ is obtained from experimental measurement. The procedure is carried out based on the following update algorithm:

$$\mathbf{x}_t = \mathbf{x}_{t-1} + \mathbf{K}_t\,[\Delta_t^{\text{meas}} - \Delta_t(\mathbf{x}_{t-1})], \tag{1}$$

where $\boldsymbol{x}_t$ is the state vector containing unknown parameters, Δ_t^{meas} is the vector containing experimentally measured displacements, and Δ_t is the exact or known displacement vector, shown as functions of state parameters. Subscript 't' represents updating increment. The correction at each increment is made through the Kalman gain matrix $\mathbf{K}_t$ which is computed as,

$$\begin{aligned}&\mathbf{K}_t = \mathbf{P}_t\boldsymbol{\delta}_t^{\mathrm{T}}\mathbf{R}_t^{-1} \quad \text{where}\\ &\mathbf{P}_t = \mathbf{P}_{t-1} - \mathbf{P}_{t-1}\boldsymbol{\delta}_t^{\mathrm{T}}(\boldsymbol{\delta}_t\mathbf{P}_{t-1}\boldsymbol{\delta}_t^{\mathrm{T}} + \mathbf{R}_t)^{-1}\boldsymbol{\delta}_t\mathbf{P}_{t-1}.\end{aligned} \tag{2}$$

Here, matrix $\boldsymbol{\delta}_t$ contains the gradients of Δ_t with respect to $\mathbf{x}_t$. $\mathbf{P}_t$ and $\mathbf{R}_t$ are the measurement covariance matrix and the error covariance matrix, respectively. Their dimensions equal to the number of measurements used in Kalman filter. For the case of FGM, there were two unknown state parameters and two measurements, and matrix $\boldsymbol{\delta}_t$ can be shown as,

$$\boldsymbol{\delta}_t = \frac{\partial \Delta_t}{\partial \mathbf{x}_t} = \begin{pmatrix} \dfrac{\partial \Delta_t^A}{\partial q} & \dfrac{\partial \Delta_t^A}{\partial n} \\ \dfrac{\partial \Delta_t^B}{\partial q} & \dfrac{\partial \Delta_t^B}{\partial n} \end{pmatrix}, \tag{3}$$

where q is the stress–strain transfer parameter and n is the power-law exponent for through-thickness variation of ceramic volume fraction. Details of these state parameters are described in Section 5.1. Also in Eq. (2), the two matrices of covariance are chosen as,

$$\begin{aligned}&\mathbf{P}_{\mathrm{o}} = \begin{pmatrix} (q_{\max} - q_{\min})^2 & 0 \\ 0 & (n_{\max} - n_{\min})^2 \end{pmatrix} \quad \text{and}\\ &\mathbf{R}_t = \begin{pmatrix} R_{t1}^2 & 0 \\ 0 & R_{t2}^2 \end{pmatrix}.\end{aligned} \tag{4}$$

Proper assignments of components are critical since they

affect the convergence characteristics of inverse analysis. In the initial matrix of measurement covariance $\mathbf{P}_o$, the diagonal components equal squares of possible ranges set for the unknown parameters. While $\mathbf{P}_o$ is diagonal, the procedure fills $\mathbf{P}_t$ to a matrix during subsequent increments. For the components of error covariance matrix $\mathbf{R}_t$, the optimal values often relates to known measurement error bounds or the maximum measurement. In the present analysis, they were set constant at $R_{t1} = R_{t2} = 0.03$ μm. This value represents approximately 1% of the indented displacement at the maximum load (i.e. 10 N) in all cases. In general, a larger value leads to slower convergence while a very small value induces instability and result in convergence to incorrect state parameters. Note that different values can be assigned at each increment when large variation occurs in the error bounds during the measurements. These assigned values in $\mathbf{P}_o$ and $\mathbf{R}_t$ produced optimal convergence characteristics during the Kalman filter process (discussed in Section 4).

3.2. Computational models for reference data

The Kalman filter compares the measured data, Δ_t^{meas}, with known solutions for a given values of state parameters. For some simplified problems, the reference solutions may be obained from closed-form analytical solutions. However, in many situations involving complex material systems, the solutions can be obtained only through separate numerical analyses. For the present problems, detailed finite element models were constructed to simulate indentation process for various specimens. Their solutions are used to form a data set where the measured data were cross-referenced in the Kalman filter during updating increments.

Fig. 4 shows a typical finite element model used in the analysis. Indented displacement reported here is obtained at the top of the hemi-spherical indenter as shown in the figure. In the actual experiments, the spherical indenter and its holder are tightly fit. Thus, any compliance differences between the finite element model and actual indenter are found to be very small (less than 0.5% of total compliance based on the detailed finite element analysis). The thickness of coating layer was modified for different test specimens of PSZ, NiCrAlY, and FGM, as were shown in Fig. 2. In addition, a larger indenter was modeled for the second FGM indentation. The model contains approximately 6600 axisymmetric four-noded isoparametric elements. In order to obtain smooth $P-\Delta$ responses, it was essential to place small elements near the contact area. In the simulation, contact condition was prescribed along the boundary between the indenter and specimen. The radius of the whole model was set large enough so that there would be no effects of outer boundary. Along the bottom of the steel substrate, nodal displacements are constrained in the vertical direction. Indentation force is gradually increased along the top surface of the indenter to simulate actual indentation tests. In the current model, small pores and voids in thermally sprayed coatings were not considered due to difficulty in modeling these micro-structural features. Any effects due to their presence are implicitly included in the overall material characteristics. Furthermore, any micro-cracks and damages, which may occur during indentation, were not taken into account. To minimize such effects on material property determination, only the loading portion of the $P-\Delta$ record was used in the inverse analysis.

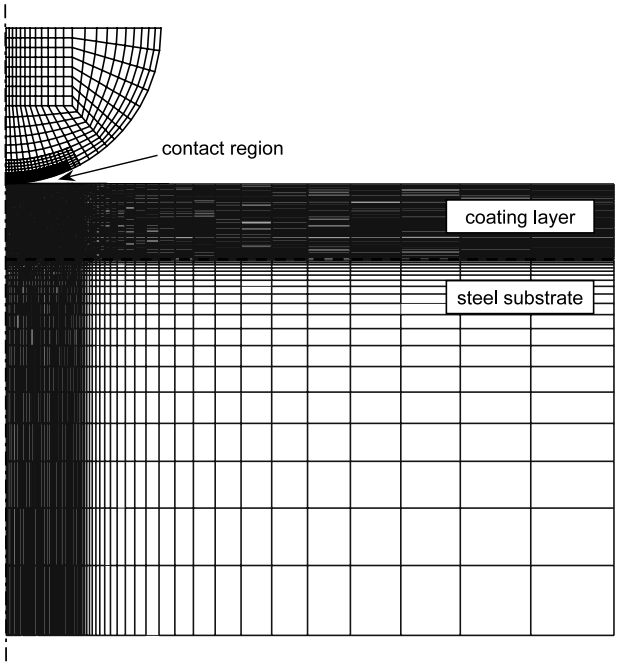

Fig. 4. A typical axisymmetrical finite element mesh for indentation simulation.

For PSZ and NiCrAlY specimens, they were modeled as homogeneous materials with pure elastic and elastic–plastic properties, respectively. For the FGM, the properties are varied along different element layers through-thickness to represent the grading. Within each layer, the material properties are prescribed according to given FGM parameters. The details of these FGM parameters are described in Section 5.1. For each specimen, possible ranges of unknown material parameters were specified. Within these ranges, finite element calculations were performed to establish the data source necessary for the inverse analysis. After the reference data was made, bi-cubic Lagrangian functions are used to interpolate the indented displacement and its gradients.

4. Characterization of homogeneous phases

Prior to testing FGM, it was necessary to determine the material properties of its constituents, PSZ and NiCrAlY, respectively. Instead of using values reported in literature, these materials were tested independently. Since the specimens were fabricated by thermal spray process, their properties can differ significantly from those in bulk or fully-dense form. Both PSZ and NiCrAlY were sprayed using the same powders and equipment as those used in the fabrication of FGM specimen. This would allow accurate and consistent evaluation of FGM parameters. In the present analysis, Poisson's ratio was assumed be known a priori or approximated. Although measurement of Poisson's ratio can be made for a homogeneous material (e.g. by ultrasound technique) [18–20], it would be difficult for FGM since it may varies through-thickness. Furthermore its role in defining the FGM characteristics is less significant than those of modulus and other parameters [21].

4.1. Determination of young's modulus for PSZ

In the present analysis, the PSZ coating was assumed to behave elastically. Thus its Young's Modulus needs to be defined. Poisson's ratio was approximated as $\nu^{\mathrm{PSZ}} = 0.25$. This leaves the Young's modulus E^{PSZ} to be the only unknown parameter to be identified. With just one unknown, the determination process was straightforward. Without using the inverse method, several finite element calculations were carried out with various values of E^{PSZ} to find the best fit to the experimentally measured P–Δ curve. Using the least-square method to minimize the differences between the numerical and measured results, we determined that $E^{\mathrm{PSZ}} = 20$ GPa represented the best match. The simulated P–Δ relation and experimentally data at selected load levels are shown in Fig. 5.

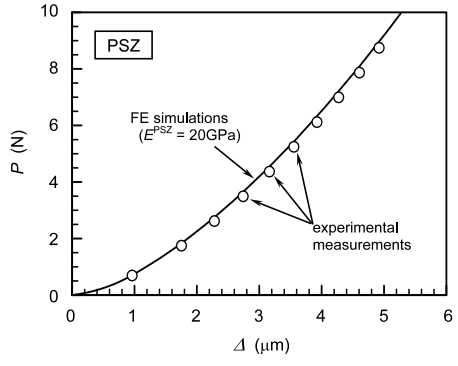

Fig. 5. Simulated load–displacement relation of PSZ with $E^{\mathrm{PSZ}} = 20$ GPa. The experimental record at selected load levels are shown with circles.

In the case of PSZ, Oliver and Pharr method [22] was also employed to extract the elastic properties from indentation. It relies on power-law fit to the unloading part of the load–displacement data. The method is based on Hertz contact theory and applicable to sharp indenters (e.g. Vickers or Berkovich) as well as smooth-profile indenters (e.g. sphere, parabolic of revolution). In this method, the composite modulus of the tested material and indenter is defined as:

$$E^* = \frac{\mathrm{d}P}{\mathrm{d}\Delta}\frac{\sqrt{\pi}}{2\sqrt{A}}, \tag{5}$$

where A and $\mathrm{d}P/\mathrm{d}\Delta$ are the contact area and the unloading stiffness at the maximum load, respectively. While the composite modulus E^* is defined by the following expression:

$$\frac{1}{E^*} = \frac{1-\nu^2}{E} + \frac{1-\nu'^2}{E'}. \tag{6}$$

E and υ are Young's modulus and Poisson ratio of the specimen, while E' and υ' are those of the indenter material. Several detailed procedures to evaluate A and $\mathrm{d}P/\mathrm{d}\Delta$ are described, for example, in Ref. [23]. Using the experimental record shown in Fig. 3(a), the Young's modulus of PSZ was estimated to be $E^{\mathrm{PSZ}} = 22$ GPa. This value is slightly higher than the one obtained from the computational model with the least-square fit. The stiffer result can be attributed to the effects of steel substrate neglected in Oliver and Pharr approach. In the finite element model, the effects of steel substrate were properly included in the indenter response.

4.2. Determination of elastic–plastic properties for NiCrAlY

Unlike PSZ, NiCrAlY is a metallic alloy and it must be modeled as elastic–plastic material. This makes the determination of its properties much more complex. Instead of using techniques introduced for homogeneous elastic–plastic materials recently [8,9,12], the inverse method proposed for FGM [13] was modified to determine its properties. First, the model for stress–strain relation was assumed to be bilinear. This choice was made since the bilinear relation was already integrated with the modified rule-of-mixture definition [2,24–26] and allows direct characterization of FGM properties in the subsequent analysis. Note, with a small modification, the present inverse method can accommodate other constitutive models such as power-law relation for homogeneous materials. In the bilinear elastic–plastic model, there are four material parameters to be defined. They are the Young's modulus, the Poisson's ratio, the yield stress and the post-yielding strain hardening ratio/modulus. As in the case of PSZ, the Poisson's ratio of NiCrAlY was assumed to be

$\nu^{NiCrAlY} = 0.25$. This leaves three parameters to be determined. In our subsequent work, the inverse analysis was extended to estimate three material parameters simultaneously. Although this procedure produced good estimates, it required more complex measurements. Essentially, to estimate more unknown parameters, P–Δ record alone was not sufficient and additional measurements such as strains were necessary. Since the present focus is determination of real FGM properties, such measurements were not carried out. Instead, Oliver and Pharr method was again used to estimate the Young's modulus of NiCrAlY. Using the unloading characteristics at the maximum load, it was determined to be $E^{NiCrAlY} = 56$ GPa. Since NiCrAlY is stiffer than PSZ, the substrate effect is likely to be less than that was observed for PSZ. The remaining two parameters are the yield stress $\sigma_o^{NiCrAlY}$ and the hardening ratio $H^{NiCrAlY}$. *Schematics of uniaxial stress–strain relation for various values of* $\sigma_o^{NiCrAlY}$ *and* $H^{NiCrAlY}$ are illustrated in Fig. 6. These parameters were estimated using the Kalman filter as described next.

The first step in the inverse analysis is to define possible ranges/domain of unknown estimates. Since likely yield stress and hardening ratio of NiCrAlY layers were unknown, the domain size was estimated by trials with reference to values reported elsewhere. After a few trials, the domain of estimates was selected as 70 MPa $< \sigma_o^{NiCrAlY} <$ 220 MPa and 6 GPa $< H^{NiCrAlY} <$ 15 GPa. Essentially the Kalman filter seeks the values of unknown parameters within this domain. Prior to performing Kalman filter with the measured P–Δ record shown in Fig. 3(a), the reference data set as described in Section 3.2 was established. Here 16 computations with various sets of $\sigma_o^{NiCrAlY}$ and $H^{NiCrAlY}$ were carried out. Their solutions and bi-cubic cubic Lagrangian interpolation functions were used to compute indented displacement and its gradients at measurement load levels. For the input of measured record, 20 load increments ranging from $P = 2.0$–9.6 N at equal increments of $\delta P = 0.4$ N were chosen. At every load increment, the Kalman filter updates the estimates until the last increment is reached. Before the Kalman filter processes the data, it requires initial estimates to be supplied. In general, final estimates are not identical for different initial estimates and some spread in converged values occurs. Since the inverse analysis technique can only provide estimates of the unknown state parameters, there is no unique method to identify the *exact solutions.* However, if the method is robust, the final values corresponding to various initial estimates should converge within small ranges of state parameters.

In the current analysis, an effective approach to obtain the *best estimates* of state variables was established. First, within the predicted domain, $\sigma_o^{NiCrAlY}$ and $H^{NiCrAlY}$ were each incremented into 41 different values. Then the Kalman filter was carried out with 1681 (i.e. 41×41) different initial estimates using the same P–Δ record. The converged locations of all the initial estimates were represented in terms of 'intensity of convergence' as shown in Fig. 7. Essentially, larger contour values signify more initial estimates converged at the particular values of $\sigma_o^{NiCrAlY}$ and $H^{NiCrAlY}$. The intensity is normalized so that the highest intensity has the value of 100. Note that a robust process leads to a small region of convergence while ill-conditioned case

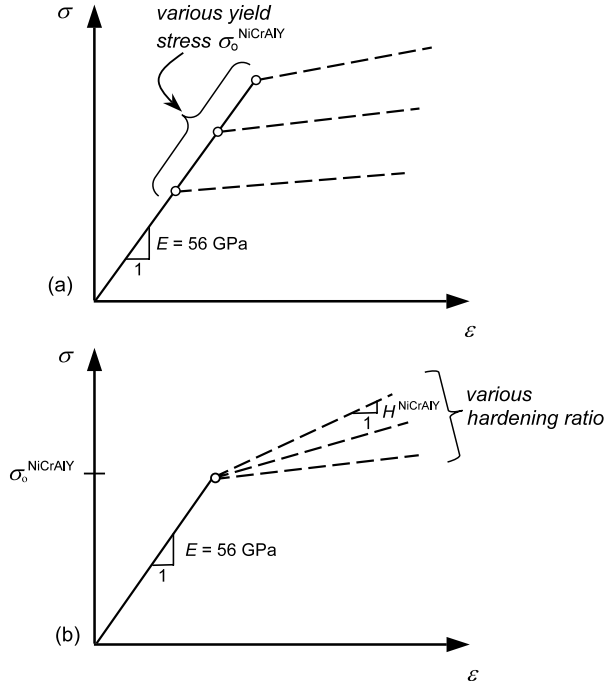

Fig. 6. Uniaxial stress–strain relations of NiCrAlY with various values of state parameters are illustrated. (a) Yield stress $\sigma_o^{NiCrAlY}$. (b) Strain hardening ratio $H^{NiCrAlY}$.

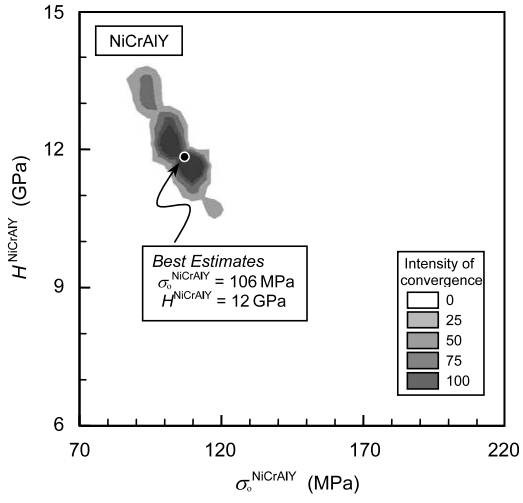

Fig. 7. Intensity of convergence plot generated from inverse analysis for NiCrAlY shown in domain of $\sigma_o^{NiCrAlY}$ and $H^{NiCrAlY}$. A high intensity represents convergence many initial estimates. The location of best estimates, found from weighted intensity, is denoted.

generates a large or many detached regions of convergence. Generally, a robust process with good convergence characteristics can be attained when there are multiple measurements and state parameters are sensitive to the measurements. Although the present analysis has only one measurement data (i.e. P–Δ record), a relatively good convergence behavior was observed. From the intensity of convergence, the best estimates were defined as where the weighted average of converged location occurred. They are $\sigma_o^{NiCrAlY} = 106$ MPa and $H^{NiCrAlY} = 12$ GPa, respectively as denoted in Fig. 7. Note among all of the initial estimates, more than 90% converged within 10% of the best estimates.

Using the best estimates obtained from the inverse analysis as inputs, the indentation on NiCrAlY coating was re-simulated with the finite element model. The resulting P–Δ relation is shown in Fig. 8 where remarkably close agreements between the simulated and measured values can be observed. The simulated results remain within the bounds of small experimental error throughout the measured time period ($0 < P < 10$ N). The close match between the simulated results and the experimental measurements supports the accuracy of the estimated $\sigma_o^{NiCrAlY}$ and $H^{NiCrAlY}$ determined from the inverse analysis.

5. Characterization of FGM

5.1. FGM parameters

Several variables are required to fully define FGM's characteristics. For the present specimen, they are the properties of individual constituents, compositional variation through-thickness and the effective properties of multi-phase at a given ratio of mixture. The properties of constituents were determined as described in Section 4.2, and the two parameters were introduced to define the latter two variables. For the compositional profile through-thickness, it was assumed that its variation to be represented by a power-law equation. With this idealization, the unknown parameter is the power exponent. According to Fig. 1, the volume fraction of PSZ phase is 80% at the top surface and 0% at the interface with the steel substrate. Thus the power-law expression for the volume fraction of PSZ is,

$$V_{PSZ} = 0.8(z/t)^n. \quad (7)$$

Here t is the thickness of FGM layer ($t = 350$ μm), z is the coordinate measured from the interface between FGM and steel substrate, and n is the power-law exponent to be sought in the inverse analysis. During fabrication process, it is difficult to precisely deposit phases to form an FGM with desired compositional profile. Synthesis of a grading profile depends on the deposition efficiency and requires integration of processing hardware, material behavior and micro-structural characteristics [14]. In general, to measure the composition variation, complex testing such as an image analysis and/or X-ray diffraction are needed. The inverse method can simplify this process. In the inverse analysis, a possible range of n was set from 1/3 to 3, which allowed a wide variation in the total content of PSZ. Any value outside this range is not usually desired since such an FGM would represent rather abrupt changes in phase content. Possible compositional variations within this

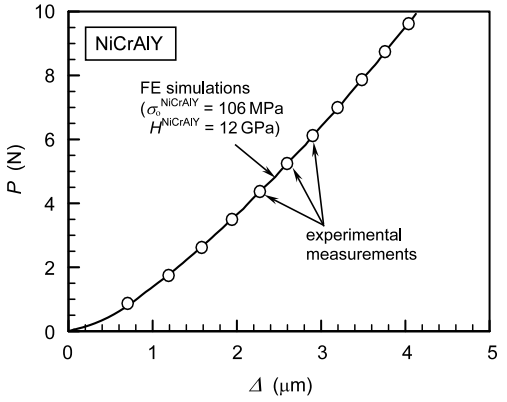

Fig. 8. Simulated load–displacement relation of NiCrAlY with estimated properties ($\sigma_o^{NiCrAlY} = 106$ MPa and $H^{NiCrAlY} = 12$ GPa). The experimental record at selected load levels are also shown with circles.

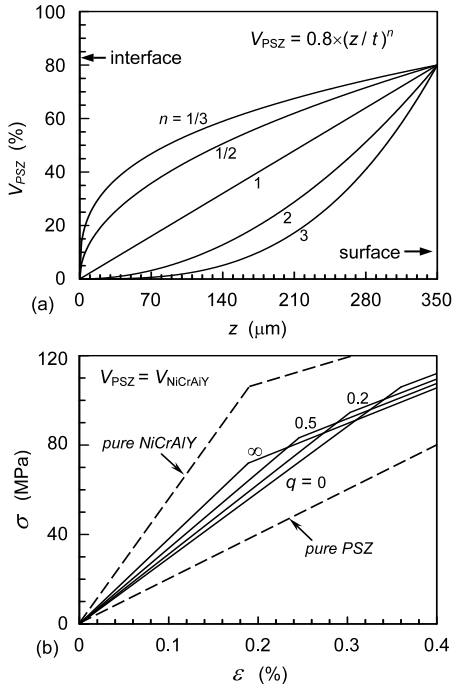

Fig. 9. Effects of two unknown FGM parameters. (a) Variations of PSZ volume fraction through-thickness ($t = 350$ μm) for various power-law exponents n. (b) Uniaxial stress–strain relations of an equal-mixture composite ($V_{PSZ} = V_{NiCrAlY}$) for various stress–strain transfer parameters q. The dashed lines correspond to pure PSZ and NiCrAlY, respectively.

range are shown in Fig. 9(a). Note in this analysis, pores and voids were not considered even though they generally represent 5–8% of the total volume. It was assumed that the effects of voids were implicitly included in the material properties as were done in the PSZ and NiCrAlY analyses earlier.

The second unknown FGM parameter defines the effective property. At a given depth of FGM coating, two phases co-exist. If the ratio of two volume fractions is known, one can approximate the effective property at this depth using rule-of-mixture model developed for composites. Here, we adopted modified rule-of-mixture [2,24–26], which uses the stress–strain transfer parameter q. Using this parameter, the thickness variation of Young's modulus can be expressed by,

$$E^{\mathrm{FGM}}(z) = \frac{E^{\mathrm{PSZ}} + \bar{V}\bar{q}E^{\mathrm{NiCrAlY}}}{1 + \bar{V}\bar{q}}, \tag{8}$$

where

$$\bar{q} = \frac{q+1}{q + E^{\mathrm{NiCrAlY}}/E^{\mathrm{PSZ}}} \quad \text{and} \qquad \bar{V}(z) = V_{\mathrm{NiCrAlY}}/V_{\mathrm{PSZ}}. \tag{9}$$

The stress–strain transfer parameter has the range of $0 \le q \le \infty$, and it essentially allows the effective property to be varied within two extreme rules-of-mixture. Reuss model is recovered when $q = 0$, and the Voigt model is assumed for $q \to \infty$. In general, q is an empirical parameter that depends on many factors including composition, micro-structural arrangement, internal constraints and others. The modified rule-of-mixture can be extended to elastic–plastic composites and the parameter q can be also used to define the effective yield stress σ_o^{FGM} and strain-hardening coefficient H^{FGM} as described in Ref. [13]. The elastic–plastic stress–strain relations of a composite with equal mixture (i.e. $V_{\mathrm{PSZ}}/V_{\mathrm{NiCrAlY}} = 1$) for various values of q are shown in Fig. 9(b). Although the effective elastic modulus shows a small variation, the yield stress can differ as much as 30% for various q's. This large span should give sufficient flexibility in estimating accurate stress–strain relations along through-thickness of FGM. In general the stress–strain transfer parameter q can be a function of relative composition (e.g. $q(V_{\mathrm{psz}})$). In our present analysis, however, q is assumed to be constant through the entire thickness and independent of the compositional ratio.

5.2. Determination of FGM parameters

According to the proposed material model, the domain of two unknown state variables n and q were set as $1/3 \le n \le 3$ and $0 \le q \le \infty$, respectively. They are large enough to accommodate a wide range of compositional variations and effective material variations. As in the case of NiCrAlY, the data source must be established to reference indented load–displacement relation for specific values of n and q prior to the Kalman filter. Here 16 sets of different n and q were selected and finite element calculation was carried out for each case to generate P–Δ relations. In the present analysis, two sets of experimental records were used simultaneously in the inverse analysis. One was from the small indenter with $R = 0.8$ mm, the other was from the large indenter with $R = 2.4$ mm as shown in Fig. 3(b). The record of second indenter provides additional information to improve the convergence characteristics. Since the Kalman filter uses the both record, 16 finite element calculations were also carried out for $R = 2.4$ mm indenter. During the inverse analysis, bi-cubic Lagrangian interpolation functions were used to compute indented displacement and its gradients at selected measurement load levels. For each indenter, 20 load increments ranging from $P = 2.0$–9.6 N, at equal increments of $\delta P = 0.4$ N, were used to update the unknown variables.

To determine the *best estimates* of n and q, the procedure described for NiCrAlY case was again followed. First, within the predicted domain, n and q were each incremented into 41 different values and the Kalman filter was carried out with 1681 different initial estimates using the same P–Δ records (of small and large indenters). The converged locations of all the initial estimates are shown in terms of the intensity of convergence in Fig. 10. Since the FGM uses two independent P–Δ records, the convergence behavior was better than that observed for NiCrAlY. A smaller region of convergence was attained and the location of best estimates can be more clearly identified. From the results shown Fig. 10, the best estimates were obtained as $q = 0.98$ and $n = 0.98$, respectively.

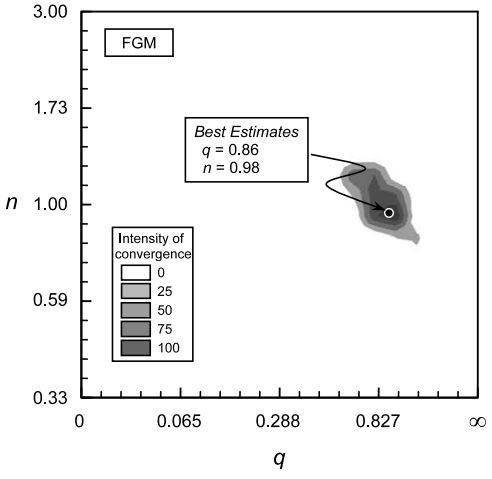

Fig. 10. Intensity of convergence plot generated from the inverse analysis for FGM. A high intensity represents convergence of many initial estimates. The location of best estimates determined from weighted average is also denoted. Note non-proportional coordinates on the axes.

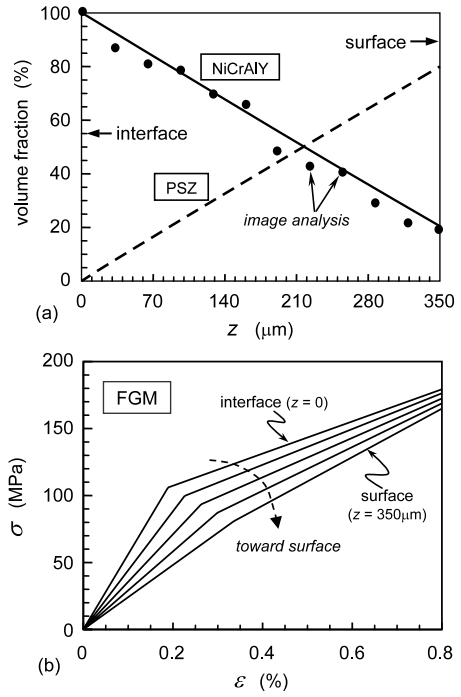

Fig. 11. FGM properties determined from the inverse analysis. (a) Through-thickness variations of PSZ and NiCrAlY volume fractions. (b) Stress–strain relations along different depths of FGM coating.

The compositional variations of PSZ and NiCrAlY through-thickness according to the best estimate are shown in Fig. 11(a). They change almost linearly with the depth of FGM coating and verify the target compositional variation of linear grading during the fabrication was precise. The varying stress–strain through-thickness was also computed from the best estimates obtained in the analysis. The stress–strain relations at various locations from the interface ($z = 0$) to the surface ($z = 350$ μm) are shown in Fig. 11(b). As the free surface is approached, the stress–strain curves become straighter to represent greater elastic response. In order to make direct comparisons with the measured P–Δ records, additional finite element calculations were carried out using these estimated compositional grading and material constants. The agreements between the measured and simulated results are excellent. For *both* indenters (with the same property inputs), the simulated results are extremely close to the experimental records during the entire loading range ($0 < P < 10$ N), shown in Fig. 12. The excellent match between the simulated results and the experimental observations strongly supports the accuracy of the estimated parameters determined from the inverse analysis.

6. Conclusions

The measurement procedure based on the inverse method proposed [13] was implemented in the real

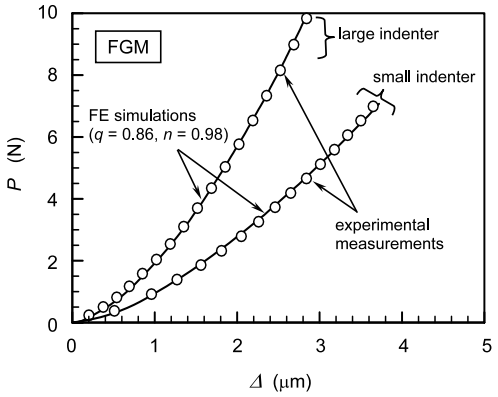

Fig. 12. Simulated load–displacement relations with estimated FGM parameters ($q = 0.86$ and $n = 0.98$) for small and large indenters. The experimental records at selected load levels are also shown with circles.

graded coating. Additional steps required for testing of actual specimens were also outlined in the present paper. This procedure allows determination of complex material parameters without resorting to extreme experimental measurements. Essentially, the inverse analysis attempts to make best estimates of unknown parameters using indirect measurements that are more easily obtainable. The Kalman filter utilized in the analysis was very suitable for the instrumented indentation where non-linear responses of materials were measured. During its recursive/updating increments, it sought for the state parameters that offered better fit to the measured data.

In addition to the application to elastic–plastic graded specimen, the inverse analysis was extended to the analysis of a homogeneous elastic–plastic material for the first time. The results obtained for NiCrAlY showed an excellent correlation between the simulated and measured values. The procedure introduced here can be applied to many classes of elastic–plastic materials. Although true values of the unknown parameters cannot be uniquely verified in any inverse analyses, an effective method was introduced to identify the best estimates. The simulated results, using the best estimates as input, produced excellent agreements with the experimentally measured records and assured high degree of accuracy. The utilization of inverse analysis allows not only the effective use of the experimental measurements but may also reduce measurement preparations. Once an instrumented indentation is set-up, the present process requires simple specimen preparation and unambiguous measurement procedure.

The steps taken in the present procedure to measure the properties of graded specimen are summarized below.

(1) Prior to testing of graded coating, pure PSZ and NiCrAlY specimens were made under similar fabrica-

tion processes. This ensures the consistency with the individual constituents in the FGM.

(2) Several indentation measurements were made with PSZ specimens and average $P-\Delta$ record was made. The Young's modulus was separately obtained by fitting finite element solutions and Oliver and Pharr method. The two results agreed well.

(3) Several indentation measurements were made with NiCrAlY specimens. First, its Young's modulus was estimated with Oliver and Pharr method. Then, the yield stress and plastic hardening ratio were determined using the inverse method and finite element solutions. Excellent agreement was observed between the measured $P-\Delta$ records and the simulated results.

(4) Several indentation measurements were made with FGM specimens using two different sized indenters. FGM parameters representing compositional variations and effective stress–strain relation through-thickness were determined using the inverse method and finite element solutions. The resulting simulations match very well with the experimentally measured $P-\Delta$ records.

A further work is underway to determine other material properties using a similar procedure. This includes fracture parameters, diffusion parameters of composites, elastic–plastic anisotropic materials. The present results based on real specimen offer promising prospects for applications of the inverse analysis to the above systems.

Acknowledgements

The work was supported by the Army Research Office under grant DAAD19-99-1-0318 and the National Science Foundation under award CMS-9800301. The authors gratefully acknowledge Professor S. Suresh for the use of the micro-indenter at M.I.T. and the assistance of K. Van Vliet during the testing. The preparation of FGM samples by G. Bancke of Center for Thermal Spray Research at Stony Brook is also acknowledged. The finite element computations were carried out using the code ABAQUS, which was made available under academic license from Hibbitt, Kalsson and Sorensen, Inc. The image analysis utilized the public software Object Oriented Finite element method (OOF), which was developed by NIST.

References

[1] S. Suresh, A. Mortensen, Fundamentals of Functionally Graded Materials, IOC Communications Ltd, London, 1998.
[2] S. Sampath, H. Herman, N. Shimoda, T. Saito, MRS Bull. 20 (1) (1995) 27.
[3] E. Weissenbek, H.E. Pettermann, S. Suresh, Acta Mater. 45 (1997) 3401.
[4] S. Suresh, A.E. Giannakopoulos, J. Alcala, Acta Mater. 45 (1997) 1307.
[5] A.E. Giannakopoulos, S. Suresh, Int. J. Solids Struct. 34 (1997) 2357.
[6] A.E. Giannakopoulos, S. Suresh, Int. J. Solids Struct. 34 (1997) 2393.
[7] G.R. Liu, X. Han, Y.G. Xu, K.Y. Lam, Compos. Sci. Technol. 61 (2001) 1401.
[8] S. Suresh, A.E. Giannakopoulos, Acta Mater. 46 (1998) 5755.
[9] A.E. Giannakopoulos, S. Suresh, Scripta Mater. 40 (1999) 1191.
[10] Y.T. Cheng, C.M. Cheng, J. Mater. Res. 14 (1999) 3493.
[11] T.A. Venkatesh, K.J. Van Vliet, A.E. Giannakopoulos, S. Suresh, Scripta Mater. 42 (2000) 833.
[12] M. Dao, N. Chollacoop, K.J. Van Vliet, T.A. Venkatesh, S. Suresh, Acta Mater. 49 (2001) 3899.
[13] T. Nakamura, T. Wang, S. Sampath, Acta Mater. 48 (2000) 4293.
[14] S. Sampath, W.C. Smith, T.J. Jewett, H. Kim, Mater. Sci. Forum 308 (1999) 383.
[15] J.S. Wallace, J. Ilavsky, J. Therm. Spray Tech. 7 (4) (1998) 521.
[16] D. Tabor, The Hardness of Metals, Clarendon Press, Oxford, 2000, p. 55.
[17] R.E. Kalman, ASME J. Basic Eng. 82D (1960) 35.
[18] P. Lasaygues, M. Pithioux, Ultrasonics 39 (2002) 567.
[19] Z.-Q. Li, X.-R. Zhang, S.-Y. Zhang, Z.-H. Shen, Compos. Sci. Technol. 61 (2001) 1457.
[20] D.A. Hardwick, Thin Solid Films 154 (1987) 109.
[21] N. Huber, A. Konstantinidis, Ch. Tsakmakis, J. Appl. Mech. 68 (2001) 218.
[22] W.C. Oliver, G.M. Pharr, J. Mater. Res. 7 (1992) 1564.
[23] A.C. Fischer-Cripps, Vacuum 58 (2000) 569.
[24] R.L. Williamson, B.H. Rabin, J.T. Drake, J. Appl. Phys. 74 (1993) 1310.
[25] A. Moretensen, S. Suresh, Int. Mater. Rev. 40 (1995) 239.
[26] S. Suresh, A. Moretensen, Int. Mater. Rev. 42 (1997) 85.